Computing ultra-precise eigenvalues of the Laplacian within polygons

Robert Stephen Jones*

Independent Researcher; Changsha, Hunan, China

The main difficulty in solving the Helmholtz equation within polygons is due to non-analytic vertices. By using a method nearly identical to that used by Fox, Henrici, and Moler in their 1967 paper; it is demonstrated that such eigenvalue calculations can be extended to unprecedented precision, very often to well over a hundred digits, and sometimes to over a thousand digits.

A curious observation is that as one increases the number of terms in the eigenfunction expansion, the approximate eigenvalue may be made to alternate above and below the exact eigenvalue. This alternation provides a new method to bound eigenvalues, by inspection.

Symmetry must be exploited to simplify the geometry, reduce the number of non-analytic vertices and disentangle degeneracies. The symmetry-reduced polygons considered here have at most one non-analytic vertex from which all edges can be seen. Dirichlet, Neumann, and periodic-type edge conditions, are independently imposed on each polygon edge.

The full shapes include the regular polygons and some with re-entrant angles (cut-square, L-shape, 5-point star). Thousand-digit results are obtained for the lowest Dirichlet eigenvalue of the L-shape, and regular pentagon and hexagon.

Keywords: Laplacian eigenvalue; Helmholtz equation; Method of Particular Solutions; point-matching method; polygon; eigenvalue bound

---

* mailto:rsjones7@yahoo.com; http://www.hbeLabs.com

INTRODUCTION

The task is to calculate very precise eigenvalues of the Laplacian within the shapes shown in Fig. 1, on which may be imposed either Neumann or Dirichlet boundary conditions.
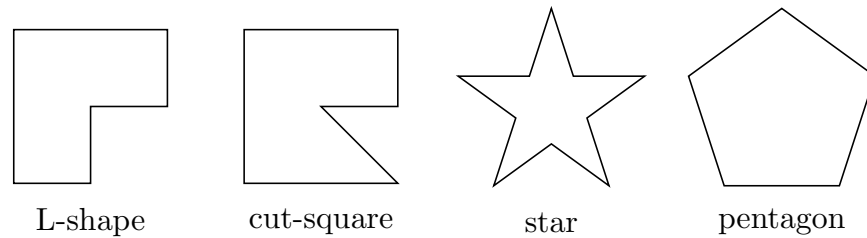

FIG. 1. Four geometries (with abbreviated names) in which a variety of Dirichlet and Neumann eigenvalues are calculated to within at least 100 digits. Of the regular polygons, only the regular pentagon is shown.

The technique is substantially identical to the method used by Fox, Henrici, and Moler [8] (hereafter referred to as "FHM") who used a method of particular solutions (MPS) called the "point-matching" or "collocation" method to calculate Dirichlet eigenvalues within the now-famous L-shape.

To see what is possible using this method, an assorted set of eigenvalues, all truncated to 100 digits of precision, for the chosen shapes (Fig. 1) is presented in Table III. In addition, three "thousand-digit" results are submitted to the "On-line Encyclopedia of Integer Sequences" [17] (OEIS.org). These results far exceed all previous published results.[1]

It is generally a good idea to plot some eigenfunctions if only to inspect the contours and nodal patterns to ensure that one is actually calculating eigenvalues. Several eigenfunction contour plots are shown in Figs. 2, 3, and 7.

(a) NB-1 (even and odd) $\lambda \approx 8.143$

(b) NC-1 (even and odd) $\lambda \approx 12.399$

(c) NB-12 (even and odd) $\lambda \approx 647.5$

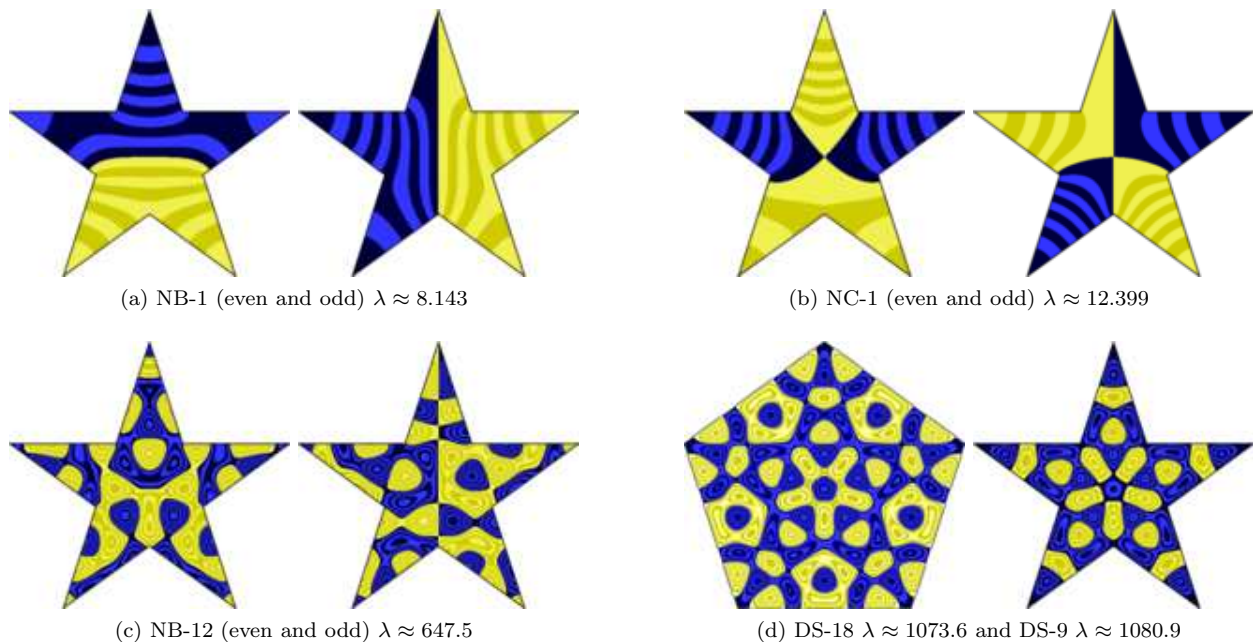(d) DS-18 $\lambda \approx 1073.6$ and DS-9 $\lambda \approx 1080.9$

FIG. 2. Example contour plots. Blue and yellow areas are opposite sign, and light-dark steps indicate level contours. (a)–(c) Three sets of degenerate Neumann star pairs. (d) (LEFT) A relatively low regular pentagon Dirichlet eigenfunction clearly revealing a *pentagram* nodal pattern, and (RIGHT) the corresponding star Dirichlet eigenfunction.

Of course, published concerns regarding the numerically ill-conditioned nature of this method must be addressed. Some such concerns were actually identified by FHM, but more recently clarified by Betcke and Trefethen [5] in

---

[1] Very recently, P. Amore, et al. [1] have independently calculated several highly precise eigenvalues (up to dozens of digits) for various shapes, including the L-shape and the cut-square. They also used the FHM method for some problems, but their focus was on a high-order Richardson extrapolation method with finite elements, which, among other things, can handle more varied shapes. Fortunately, their calculations provide (partial) independent validation of my results.

2004, when they demonstrated the numerical advantages of the so-called "generalized singular-value decomposition" (GSVD) method, a relative to the point-matching method.

Fortunately, the answer to make the point-matching method work is short and simple: One must both (a) select adequate matching points (both number and distribution) and (b) keep enough precision in the intermediate calculations. My empirical observations are that Chebyshev nodes chosen as matching points (as suggested by Betcke and Trefethen [5]) often work well, even where equally-spaced points do not, and the precision of the intermediate calculations must be significantly higher, often several times, than the precision of the eigenvalue.

(a) DC-27 (even and odd) $\lambda \approx 1044.72$ (b) DS-65: $\lambda \approx 4293.91$ (c) DS-1396: $\lambda \approx 100001.28$
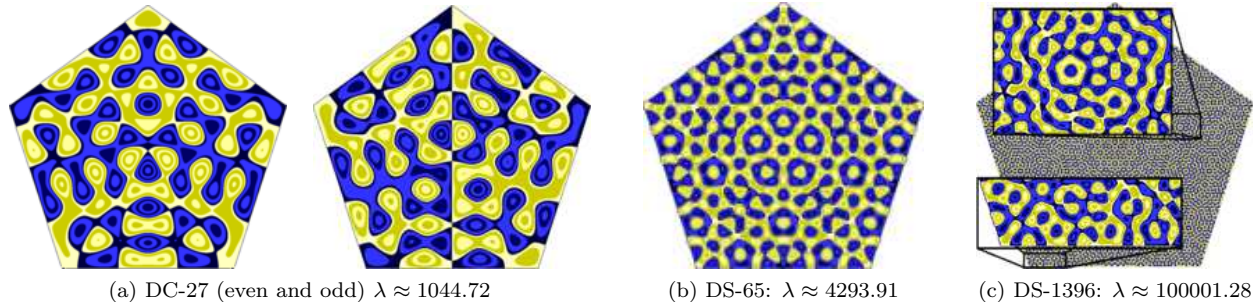
FIG. 3. Several representative Dirichlet eigenfunctions within the unit-edged regular pentagon. Blue and yellow areas are opposite sign, and light-dark steps indicate level contours. (a) The degenerate pair just below DS-18 (see Fig. 2d, LEFT). (b) Another example that strongly reveals the *pentagram* nodal pattern. (c) The first eigenfunction with eigenvalue above 100,000, corresponding to the 8139th overall eigenvalue, and having about fifty wavelengths along a pentagon edge ($\Lambda \approx 0.020$). Notice how the boundary shape is revealed within the sea of apparent chaos (upper inset). See Eq. (45) for an abbreviated 300-digit eigenvalue bound.

The ability to calculate many digits depends on the convergence rate, and a good way to improve it is to exploit symmetries. Fortunately, this exploitation has the important side-effects of (a) reducing the complexity of the region in which one must work, (b) classifying eigenmodes, and (c) disentangling geometrically degenerate eigenfunctions. Do not underestimate the importance of exploiting symmetry.

At virtually every step in this project, only free software[2] running on modern commodity computer hardware has been used, and with great success. The software of choice is the `GP/PARI` calculator [19] using the GNU Multiple Precision Arithmetic Library `gmp` [9] running on a laptop computer with a `GNU/linux` operating system and its countless ancillary programs. (Some use was also made of `maxima` [14] for the occasional symbolic calculation.) This programming environment permits efficient numerical computations while "natively" retaining up to several thousand digits of precision.

Several personal computers were used, but the best was a modern laptop computer with 16 GB RAM and a quad-core i7 processor with eight threads.[3] CPU times are reported using that laptop, and are unavoidably approximate due to multitasking.

Before beginning, it should be made clear that this is a classical and very well-known problem, worked on by many people over the last two-hundred years—with many applications and results. As such, I shall limit the discussion to only those facts that are required to reproduce and possibly extend the present calculations. A thirty-year-old, but still popular and relevant survey of the problem was given by Kuttler and Sigillito [12]. More practically, active investigators, Barnett and Betcke have created `MPSpack` [2, 3] that helps bring sophisticated eigenvalue calculations closer to the rest of us.

Despite the long history, except for the recent work of P. Amore, et al. [1] , who incidentally make this same observation, I am unaware of any published, non-closed-form eigenvalues accurate to just beyond a dozen or so digits for *any* shape not related to the closed-form solutions within the equilateral triangle, rectangle, or circle (ellipse). All eigenvalue results in this report are likely unprecedented.

THE EIGENVALUE PROBLEM

Let $\mathbf{r}$ be a point in the plane described by either Cartesian coordinates "(x, y)" or polar coordinates "(r, θ)", where $x = r \cos \theta$ and $y = r \sin \theta$, and where notation ambiguity is removed by context. The two-dimensional Helmholtz

---

[2] Typically per the GPL http://www.gnu.org/philosophy/free-sw.html.
[3] At times, using up to 50 GB swap space.

equation is

$$\Delta\Psi(k;\mathbf{r}) + \lambda\Psi(k;\mathbf{r}) = 0 \tag{1}$$

where Δ is the Laplacian and $k = \sqrt{\lambda}$ is the usual "wavenumber". Without a boundary, λ (or k) is treated as a continuous eigen-parameter, and $\Psi(k;\mathbf{r})$ may describe a free wave with wavelength $\Lambda = 2\pi/k$. The "interior" Helmholtz eigenvalue problem is obtained by restricting $\mathbf{r}$ to the interior of a region (one of Fig. 1), and imposing relevant boundary conditions (Neumann or Dirichlet), which constrains λ to a non-accumulating set of discrete eigenvalues, some of which may be degenerate. (The trivial, "closed-form", Neumann solution, i.e., $\Psi = $ constant with $\lambda = 0$, is completely ignored in this project.)

The point-matching method works if the eigenvalues are non-degenerate. Thus it is very important to deal with degeneracies either by (a) dismissing them or (b) disentangling them using symmetry.

First, closed-form solutions are not only known[4], but also arbitrarily high in "accidental" degeneracy as one climbs the eigenvalue towers[5]; so after identifying them, simply exclude them from the calculations.

Second, if there is a geometric or reflection symmetry, all eigenfunctions can be sorted into separate symmetry classes—some of which may be closed-form. Doing so effectively splits the problem up into a set of sub-problems, each one with a corresponding symmetry-reduced polygon and edge conditions, and a resulting, non-accumulating, infinite tower of distinct eigenvalues

$$0 < \lambda_1 < \lambda_2 < \lambda_3 < \cdots < \lambda_\alpha < \cdots, \tag{2}$$

where α labels the eigenvalue within that tower. Considering only the non-closed-form symmetry classes, it is indeed assumed that there are no degeneracies within such a tower.[6] Thus, to each non-closed-form symmetry class, we associate a sub-problem, effectively consisting of non-degenerate eigenmodes. A tower of such eigen-pairs for a given symmetry class shall be written as the set

$$\{\lambda_\alpha, \Psi_\alpha(\mathbf{r}) \,|\, \alpha = 1, 2, 3, ...\} \tag{3}$$

where $\Psi(k_\alpha;\mathbf{r}) \equiv \Psi_\alpha(\mathbf{r})$. Degeneracies, of course, may exist between separate symmetry classes, so it may be possible to choose a subset of non-closed-form classes and calculate only those eigenvalues.

It is these symmetry-reduced, sub-problems that we focus on. In the end, one can piece together all of the eigenmodes of each symmetry class to construct the complete spectrum for the chosen shapes in Fig. 1, which restores the rich assortment of symmetries and degeneracies. See, for example, Fig. 10 depicting the lowest seventy-nine eigenvalues of the star.

As is conventional, an edge or a line of symmetry within the shape is said to be "even" or "odd" according to how a corresponding eigenfunction transforms under Riemann-Schwarz reflection. Also, for the purposes of this report, the analyticity of a vertex is defined by whether or not an eigenfunction can be (locally) Riemann-Schwarz reflected around that vertex and remain single valued.[7]

In the current project, not all boundary edges will be either even or odd. Indeed, types of symmetry arise where (a) the eigenfunction satisfies a periodic-like condition such that values along one edge are proportional to values along another edge (star and regular polygon), or (b) a reflection symmetry may be exploited, effectively excluding terms from the eigenfunction expansion (L-shape and cut-square).

To demonstrate the technique, it is necessary to introduce a polygon, Ω, as illustrated in the example of Fig. 4. The specific form of Ω depends on the symmetry group of the problem, and for this project, define it to be an s-sided polygon with at most one non-analytic vertex from which all edges can be seen. Label the vertices V_a, where $a = 1, 2, ..., s$; beginning with the non-analytic vertex and proceeding clockwise. (In the example, $s = 4$.) The edges are labeled similarly, specifically, $\partial\Omega_a$ connects V_a to V_{a+1} (mod s, as required). The "adjacent" edges are $\partial\Omega_1$ and $\partial\Omega_s$, while the "point-matched" edges are $\partial\Omega_a$, where $a = 2, 3, ..., s-1$. In this project, the shapes are such that only the adjacent edges lie along lines passing through the non-analytic vertex.

Define the *canonical position* of Ω as follows. First locate the non-analytic vertex, V_1, at the origin, and orient as needed so that $\partial\Omega_1$ and $\partial\Omega_2$ are independently even or odd. Then, rotate around V_1 until $\partial\Omega_2$ is parallel to the y-axis at a positive x-value. In this canonical position, each edge $\partial\Omega_a$ is a segment of the line

$$\mathcal{L}_a : A_a x + B_a y = C_a \tag{4}$$

---

[4] Among the chosen shapes, the L-shape, cut-square, and regular hexagon have subsets of closed-form solutions. For polygons, a closed-form solution can be written as a finite sum of plane waves, and its eigenvalue is related to π, presently known to 13.3×10^{12} digits.

[5] This is related to the increasing number of integer solutions to Diophantine equations $a^2 = b^2 + c^2$ (rectangle) and $a^2 = b^2 + bc + c^2$ (equilateral triangle).

[6] Such non-closed-form degeneracies are possible but presumably quite rare. This assumption should be independently verified.

[7] All non-closed-form solutions in this project have an Ω with exactly one non-analytic vertex. For all eigenfunctions within a given symmetry class, it seems that a vertex will be either analytic or not.

where the constants (A_a, B_a, C_a) are uniquely chosen by requiring that

$$\widehat{\mathbf{r}}_{n,a} = A_a\widehat{\mathbf{x}} + B_a\widehat{\mathbf{y}} \tag{5}$$

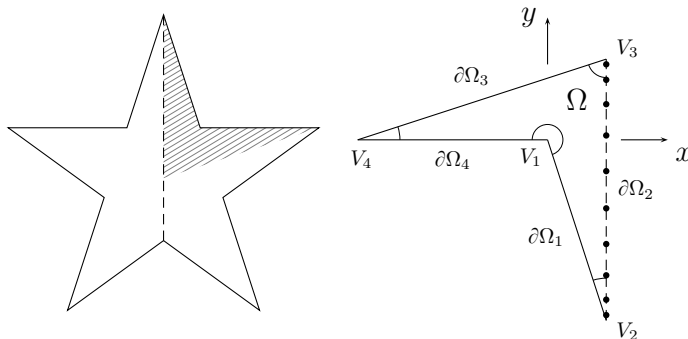be an outward pointing unit normal.

FIG. 4. (LEFT) Star shape showing how (RIGHT) an arrowhead polygon, Ω, in its canonical position, is constructed for the $\mathcal{B}_e$ and $\mathcal{C}_e$ eigenfunctions of the star. The vertical bisector of the star for these eigenfunctions is an even (dashed) line, a portion of which becomes $\partial\Omega_2$. Edges $\partial\Omega_1$ and $\partial\Omega_4$ have same boundary conditions as the star, while edge $\partial\Omega_3$ satisfies a periodic-type boundary condition (values on $\partial\Omega_3$ are proportional to corresponding values on $\partial\Omega_2$). Also shown are $N/2 = 10$ Chebyshev distributed matching points on $\partial\Omega_2$. The other $N/2$ points would be symmetrically located on Ω_3. V_1 is non-analytic for all symmetry classes of the star.

The two adjacent edges, $\partial\Omega_1$ and $\partial\Omega_s$, at polar angles ϕ_1 and ϕ_s, respectively, form the non-analytic vertex, which has internal angle

$$\Delta\phi = \phi_s - \phi_1. \tag{6}$$

It is also convenient to introduce the abbreviation,

$$\tilde{\theta} \equiv \theta - \phi_1 \tag{7}$$

Having stated the problem, with some specific restrictions and conventions, the next task is to describe the method of solution, the so-called "point-matching" method.

THE POINT-MATCHING METHOD

Precisely following FHM, expand the eigenfunction in a truncated Fourier-Bessel series

$$\Psi^{[N]}(k;\mathbf{r}) = \sum_{\nu=1}^{N} c_\nu^{[N]} \, \psi_\nu(k;\mathbf{r}) \tag{8}$$

where the so-called "basis functions" are

$$\psi_\nu(k;\mathbf{r}) = J_{m_\nu}(kr) \times \begin{cases} \sin(m_\nu\tilde{\theta}), & \partial\Omega_1(\text{odd}) \\ \cos(m_\nu\tilde{\theta}), & \partial\Omega_1(\text{even}) \end{cases} \tag{9}$$

where, as indicated, the choice is based solely on if the adjacent edge $\partial\Omega_1$ is odd or even; and $J_m(x)$ is the Bessel function of the first kind of order m.[8] The index ν runs from 1 to N, here labeling the term in the expansion; and the m_μ are not yet specified.

When the symmetry requirements and boundary conditions are enforced along *both* adjacent edges, the m-values are restricted. It often happens that the adjacent edges are independently even or odd, in which case, the m-values

---

[8] To calculate only eigenvalues, we need not normalize these basis functions.

are given by

$$
m_\nu = \frac{\pi}{\Delta\phi} \times \begin{cases} (\nu - 1) & \text{both even} \\ (\nu - \frac{1}{2}) & \text{one odd, other even} \\ \nu & \text{both odd} \end{cases} \tag{10}
$$

Among the chosen shapes, the L-shape and cut-square have other interesting symmetry-related restrictions on the m-values due to the fact that these shapes can be obtained by reflecting a 45-90-45 triangle, respectively, six and seven times.

Once the required m-values are selected, it is important to realize that $\Psi^{[N]}(k; \mathbf{r})$ is an *exact* solution within the infinite sector $\phi_1 \le \theta \le \phi_2$. This is true for any positive integer N and real $\lambda = k^2 > 0$ (excluding $\lambda = 0$). The function $\Psi^{[N]}(k; \mathbf{r})$ is specifically crafted to handle the non-analyticity of V_1 and the boundary or symmetry conditions on the adjacent edges $\partial\Omega_1$ and $\partial\Omega_s$, exactly.

The above formalism generally applies to the MPS. The next step, unique to the "point-matching" method, is to select N points,

$$
\mathcal{P}_N : \{ \mathbf{r}_\mu \,|\, \mu = 1, 2, 3, \cdots, N \} \tag{11}
$$

on the non-adjacent edges where the edge conditions may be nontrivially enforced on those edges.[9] This is the same N that appears in the eigenfunction expansion, Eq. (8). Selecting adequate sets of matching points is a nontrivial task that is key to making the point-matching method work. For the immediate following, assume this has been done.

Enforcing the boundary conditions or symmetry-related edge conditions at the N matching points yields N linear equations in the N expansion coefficients (the $c_\nu^{[N]}$ in Eq. (8)), and a resulting $N \times N$ "point-matching matrix", $\mathcal{M}^{[N]}(\lambda)$. Linear algebra suggests that the determinant of this matrix must be zero for nontrivial solutions to exist, i.e.,

$$
\left| \mathcal{M}^{[N]}(\lambda) \right| = 0 \tag{12}
$$

This is the so-called "point-matching determinant", and finding roots of this equation for increasing values of N is the name of the game.

For a given N, there is an infinite number of roots of the point-matching determinant, but only the first κ_N of them,

$$
0 < \lambda_1^{[N]} < \lambda_2^{[N]} < \cdots < \lambda_{\kappa_N}^{[N]} \tag{13}
$$

are guaranteed to correspond to actual eigenvalues. The number κ_N is such that if N is increased to $N + \Delta N$, this set of roots may become better estimates of the eigenvalues, but new roots may be introduced only for values of λ a little bigger than $\lambda_{\kappa_N}^{[N]}$.

Thus, for a given eigenvalue, λ_α, there is a minimum N-value, say $N_{\alpha,1}$, above which Eq. (12) may yield increasingly better estimates as N is incremented. I conjecture that a more detailed picture shall require $N_{\alpha,1}$ be big enough so that a gently "wiggling" contour passes continuously through all the matching points—a contour along which the edge conditions are satisfied exactly.[10]

The smallest, problem-dependent value of ΔN defines a "properly incremented" set of N-values, say $\{N_\alpha\}$, where its members are

$$
N_{\alpha,i} = N_{\alpha,1} + (i - 1)\Delta N \qquad i = 1, 2, 3, \cdots; \tag{14}
$$

that yield a corresponding set of approximate eigenvalues

$$
\left\{ \lambda_\alpha^{[N_{\alpha,1}]}, \lambda_\alpha^{[N_{\alpha,2}]}, \lambda_\alpha^{[N_{\alpha,3}]}, \cdots \right\}. \tag{15}
$$

Provided everything "works", we then tacitly assume that the approximate eigen-pair converges to the corresponding

---

[9] For example, if $\partial\Omega_1$ and $\partial\Omega_2$ are both odd, then V_2 cannot be used as a matching point.

[10] For example, if the point-matched edge is odd, then that contour would be a nodal curve passing through the matching points. If N is too small for a given eigenvalue, then, for example, two adjacent matching points might not be directly joined by nodal curve, although nodal curves will pass through those matching points.

exact eigen-pair (see Eq. (3)), specifically,

$$\lim_{N \to \infty} \left\{ \lambda_\alpha^{[N]}, \Psi^{[N]}(k_\alpha^{[N]}; \mathbf{r}) \right\} = \{\lambda_\alpha, \Psi_\alpha(\mathbf{r})\} \tag{16}$$

where $N \in \{N_\alpha\}$. The procedure depends on several factors, most notably, the nature of the vertices and the distribution of the matching points.

EIGENVALUE BOUNDS

If the rate of convergence is "exponential", a very interesting thing happens that might be used to obtain eigenvalue bounds, by inspection. Specifically, the problem may be set up so that that sequence of approximate eigenvalues, Eq. (15), as N increases, can be made to alternate above and below an asymptote—assumed to correspond to an eigenvalue—in such a way that the peaks of that alternation effectively provide an increasingly narrow bound for that eigenvalue.[11] This means we can write

$$\lambda_\alpha^{[N_\downarrow]} < \lambda_\alpha < \lambda_\alpha^{[N_\uparrow]} \tag{17}$$

where $N_\downarrow$ and $N_\uparrow$ correspond to N-values of a given minimum and the previous or next maximum, respectively. Table I clearly illustrates that alternation for the L-shape calculation—not only for my modern calculation, but (interestingly) also for the original FHM data.

To calculate many digits, one must estimate the roots of the point-matching determinant, Eq. (12), to a precision somewhat higher than the observed bound, Eq. (17), at a given N-value. By construction, the eigenvalues are not degenerate, meaning the point-matching determinant only has simple roots, so it is actually quite straightforward to calculate those roots to very high precision.[12] This key ingredient—the ability to precisely locate those roots—is a significant advantage of the point-matching method over some other methods, like the GSVD method (which seeks minima of a function).

Another important feature of the point-matching method is that the number of basis functions is maximized for a given number of matching points. With more terms, the approximate eigenfunction better matches the exact eigenfunction.

With a given eigenvalue bound in hand, there are several related and useful numbers one can calculate. They are (a) the relative gap, (b) the approximate number of correct digits, and (c) the global convergence rate; respectively,

$$(a) \quad \epsilon_\alpha^{[\widehat{N}]} = \frac{\lambda_\alpha^{[N_\uparrow]} - \lambda_\alpha^{[N_\downarrow]}}{\frac{1}{2}\left[\lambda_\alpha^{[N_\uparrow]} + \lambda_\alpha^{[N_\downarrow]}\right]} \qquad (b) \quad D_\alpha^{[\widehat{N}]} = -\log_{10}\left(\epsilon_\alpha^{[\widehat{N}]}\right) \qquad (c) \quad \rho_\alpha^{[\widehat{N}]} = \frac{D_\alpha^{[\widehat{N}]}}{\widehat{N}} \tag{18}$$

where the $\widehat{N} = \max(N_\uparrow, N_\downarrow)$ form a new set of N-values, $\{\widehat{N}_\alpha\}$, a subset of $\{N_\alpha\}$.

Note that Eqs. (18) provide a practical, numerical definition of what it means to be "exponentially convergent". Such a practical definition is useful since the exact value of the eigenvalue is never really known. Specifically, if $\rho_\alpha^{[\widehat{N}]} = \rho_\alpha$ is constant wrt $\widehat{N}$, then the eigenvalue *relative gap* decays exponentially, i.e.,

$$\epsilon_\alpha^{[\widehat{N}]} \sim 10^{-\rho_\alpha \widehat{N}} \tag{19}$$

as $\widehat{N} \to \infty$. My observation is that the global convergence rate ρ for non-closed-form solutions is typically a decreasing function of $\widehat{N}$.

Convergence rates that permit relatively easy 100-digit results range down to about 1/6 or so, and the best convergence rates for the chosen shapes are typically a little better than 1/2. Note that this reciprocal notation is useful because it reveals how many matching points—or terms in the expansion—must be added to achieve each additional eigenvalue digit: Thus, if $\rho = 1/4$, then four additional terms in the expansion and a corresponding four additional matching points will add an additional eigenvalue digit.

---

[11] I first observed this alternation property in 1993 [11] with exponentially-convergent closed-form solutions.

[12] The point-matching determinant changes sign as one passes a root, i.e., provided that $\delta\lambda$ is sufficiently small, then if "$|\mathcal{M}(\lambda)| \times |\mathcal{M}(\lambda + \delta\lambda)| < 0$", then the root is in the interval $(\lambda, \lambda + \delta\lambda)$. Without knowing the smallest gap between eigenvalues, it is important to independently locate each eigenvalue. The GSVD method is perhaps better suited to sweep an interval to locate eigenvalues.

To report a bound, suffix the matching digits with a rounded-up superscript and a rounded-down subscript. This conservative approach helps ensure that the reported bound will include the true eigenvalue. To illustrate, consider the relatively difficult-to-calculate, lowest Dirichlet eigenvalue within a 256-sided regular polygon (area=π). It is first precisely calculated to

$$\lambda = \begin{cases} 5.7831876203689428757289266\mathbf{1}... & \text{for } N_\downarrow = 930 \\ 5.7831876203689428757867165\mathbf{8}... & \text{for } N_\uparrow = 929 \end{cases} \tag{20}$$

This calculation used $N = 282, 283, ..., 929, 930$; while judiciously skipping N-values, and stopping when $\epsilon < 10^{-20}$. Very reliably, even and odd N-values provided lower and upper bounds, respectively. From that result, one may write the bound

$$\lambda = 5.7831876203689428757^{868}_{289} \tag{21}$$

for $\widehat{N} = 930$. For this example, $\epsilon = 9.99 \times 10^{-21}$, $D = 20.00$, and $\rho = 1/46.5$. To get that twenty-digit result took almost two CPU days. Despite achieving *only* twenty digits, this example does exhibit exponential convergence. Indeed, more detailed inspection reveals the relationship

$$\epsilon^{[\widehat{N}]} \approx 10^{-\left(5.73 + \widehat{N}/65.1\right)} \tag{22}$$

based on $280 \leq \widehat{N} \leq 930$, which specifically indicates exponential convergence.[13] Incidentally, for comparison, the best "published" value may be calculated with Eq. (43), yielding $\lambda \approx \underline{5.783187620368946}869....$, of which the first fifteen (underlined) digits appear to be correct. I am unaware of any efforts to calculate this particular eigenvalue.

Note that above a few dozen eigenvalue digits, either the "correct digits" (e.g., 5.78...28757) or the "correctly rounded digits" (e.g., 5.78...2876) may seem more impressive than the actual bound. But the bound is nevertheless useful because the exact value is not known, and one may not know otherwise where to stop counting correct digits.

It is the alternation property that provides the bounds, but what causes that alternation? By considering the necessary continuous contour through the matching points along which the boundary or symmetry conditions are satisfied exactly, I offer a simple heuristic explanation.[14] Such a contour defines an area A_N in which $\{\lambda_\alpha^{[N]}, \Psi^{[N]}(k_\alpha, \mathbf{r})\}$ is an *exact* solution. As matching points are added, that area not only approaches the polygon area, A, but I conjecture that the contour "flips", analogous to "$\sin \to -\sin$"; and that such a flipping causes the area to alternate above and below the polygon area. Since the area difference is very small[15], using $\lambda_\alpha^{[N]} A_N \approx \lambda_\alpha A$, it becomes plausible that such a flipping causes the alternation.

My empirical observation is that if there is exponential convergence, then it becomes more likely that flipping occurs with each proper increment the closer the matching-point distribution is to being equally-spaced. More optimal (or necessary) Chebyshev distributions give better convergence rates, but quite often require several proper increments to flip. In that case, the number of proper increments is often irregular, but may become more regular for higher N-values. Any automatic program should make sure that what appear to be upper and lower limits are actually so.

Note that this eigenvalue bounding technique is related to, but slightly different from the conventional approach of using the approximate eigenfunction along the point-matched edges, as in the Moler-Payne method [15]. A practical difference is that one need not calculate the coefficients (to evaluate the eigenfunction along the point-matched edges) to calculate the upper and lower limits to the eigenvalue. Instead, the eigenvalue bound here is identified by "simply" watching roots of the point-matching determinant as N is increased. However, ease of calculation may not be the only advantage: It may indeed provide *better* bounds, as demonstrated with the L-shape calculation below.

To make all of this work well, one must identify symmetries, select polygons and adequate matching point distributions, and calculate precise values of the point-matching determinant for a properly incremented set of N-values. For a given problem, this may be an iterative procedure as one discovers new things.

THE MATCHING POINTS

Next consider the nontrivial task of choosing matching points. Each problem will have a specific choice, but there are some common strategies. Suppose each point-matched edge $\partial\Omega_a$ has n_a matching points at which the edge

---

[13] Going from $\widehat{N} = 280 \to 930$, the global convergence rate decreases from $1/27.9 \to 1/46.5$. Asymptotically, $\rho^{[\widehat{N}]} \sim 1/65.1$.

[14] This is certainly not a mathematical proof, but is quite plausible.

[15] The area difference for a 100-digit eigenvalue is $\Delta A/A = 10^{-100}$: Whimsically compare the area of a drum (vibrating membrane) with a diameter matching that of the universe, i.e., $R = 47 \times 10^9 \ell y$, $A = 6.1 \times 10^{53} \text{ m}^2$, to the area change equal to the cross-sectional area of a proton, i.e., $R = 0.88 \text{ fm}$, $\Delta A = 2.4 \times 10^{-30} \text{ m}^2$. This $\Delta A/A = 4.0 \times 10^{-84}$ is some fifteen orders of magnitude larger.

conditions may be nontrivially satisfied.

For the point-matching method to work well, it is somewhat important that—as N is incremented—the same proportion of matching points be used on each edge, and the spacing and distribution should also be approximately similar on each edge. These requirements help define a "proper increment", Eq. (14).

It is also recommended that the maximum gap between matching points is always smaller than some empirically determined fraction of the free wavelength, $\Lambda = 2\pi/k$. This will help ensure that the contour connecting matching points does indeed pass continuously through all the matching points.

Equally-spaced matching-points seem quite popular and easy to program, but these do not always work and are certainly not the best. It seems that crowding points near vertices is good practice since that is usually where the contour tends to deviate from the polygon edge the most: Crowding the points constrains the contour better.

Chebyshev nodes usually yield excellent results and happen to be quite easy to program. Indeed, let $s = 0$ to ℓ measure the position along a point-matched edge $\partial\Omega_a$, then

$$s_\mu = \frac{\ell}{2}\left[1 - \cos\left(\frac{\mu - \frac{1}{2}}{n_a}\pi\right)\right] \tag{23}$$

where $\mu = 1, 2, 3, ..., n_a$ is a canonical set of Chebyshev nodes. This distribution has points very close to the end-points, and a relative crowding near those end-points. Variations may be used, for example, to ensure more crowding near acute, distant vertices.

THE POINT-MATCHING MATRIX

Armed with an adequate selection of matching points, the next task is to describe the matrix elements. Each point-matched edge, $\partial\Omega_a$ with n_a matching points, can be odd, even, or satisfy a periodic-type requirement; and each will yield n_a rows of the point-matching matrix.

Odd point-matched edge

If the point-matched edge $\partial\Omega_a$ is odd, the n_a rows are obtained by equating $\Psi^{[N]}(k; \mathbf{r})$ at the n_a matching points to zero. Specifically,

$$\Psi^{[N]}(k; \mathbf{r}_\mu) = 0 \qquad \mathbf{r}_\mu \in \partial\Omega_a(\text{odd}), \tag{24}$$

which yields n_a rows,

$$\mathcal{M}^{[N]}_{\mu\nu}(\lambda) = J_{m_\nu}(kr_\mu) \times \begin{cases} \sin(m_\nu\tilde{\theta}_\mu), & \partial\Omega_1(\text{odd}) \\ \cos(m_\nu\tilde{\theta}_\mu), & \partial\Omega_1(\text{even}) \end{cases} \tag{25}$$

The vast majority of published accounts of all variants of the MPS use Dirichlet boundary conditions, so this is perhaps a well-known result. It is also relatively easy to program.

Even point-matched edge

If the point-matched edge $\partial\Omega_a$ is even, the formulas are also elementary and easy to program, but a little long. These results appear to be less well-known, so they may be of some utility.

First recall equations (4) and (5), which define a line—a segment of which forms edge $\partial\Omega_a$—and an "outward-pointing" unit normal, $\widehat{\mathbf{r}}_{n,a}$. Equating the normal derivative of $\Psi^{[N]}(k; \mathbf{r})$ at the n_a matching points to zero shall yield the corresponding n_a rows of the matrix. Specifically,

$$\left.\frac{\partial\Psi^{[N]}(k; \mathbf{r})}{\partial r_{n,a}}\right|_{\mathbf{r}_\mu} = 0 \qquad \mathbf{r}_\mu \in \partial\Omega_a(\text{even}) \tag{26}$$
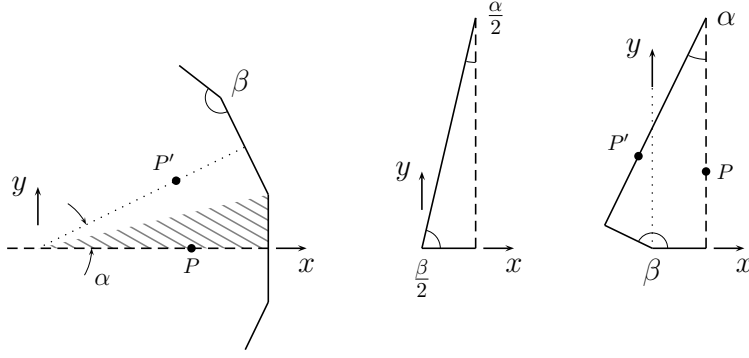
FIG. 5. (LEFT) A regular polygon with an even apothem (dashed) on the positive x-axis, (CENTER) the triangular fundamental region, and (RIGHT) the kite-shaped region for the doubly degenerate eigenmodes. Values of an even (Q-parity), doubly-degenerate eigenfunction are proportional to each other at points P and P'.

where

$$\frac{\partial \Psi}{\partial r_{n,a}} = A_a \frac{\partial \Psi}{\partial x} + B_a \frac{\partial \Psi}{\partial y}. \tag{27}$$

To make the formulas less cumbersome, split $\mathcal{M}$ into two $N \times N$ matrices, $\mathcal{X}$ and $\mathcal{Y}$, such that

$$\mathcal{M}_{\mu\nu}^{[N]} = A_a \mathcal{X}_{\mu\nu}^{[N]} + B_a \mathcal{Y}_{\mu\nu}^{[N]}. \tag{28}$$

Differentiating the basis functions and evaluating at the matching points yields

$$r_\mu^2 \mathcal{X}_{\mu\nu}^{[N]}(\lambda) = \begin{cases} m_\nu \left[x_\mu \sin(m_\nu \tilde{\theta}_\mu) - y_\mu \cos(m_\nu \tilde{\theta}_\mu) \right] J_{m_\nu}(kr_\mu) - kr_\mu x_\mu \sin(m_\nu \tilde{\theta}_\mu) J_{1+m_\nu}(kr_\mu), & \partial\Omega_1(\text{odd}) \\ m_\nu \left[x_\mu \cos(m_\nu \tilde{\theta}_\mu) + y_\mu \sin(m_\nu \tilde{\theta}_\mu) \right] J_{m_\nu}(kr_\mu) - kr_\mu x_\mu \cos(m_\nu \tilde{\theta}_\mu) J_{1+m_\nu}(kr_\mu), & \partial\Omega_1(\text{even}) \end{cases} \tag{29a}$$

$$r_\mu^2 \mathcal{Y}_{\mu\nu}^{[N]}(\lambda) = \begin{cases} m_\nu \left[x_\mu \cos(m_\nu \tilde{\theta}_\mu) + y_\mu \sin(m_\nu \tilde{\theta}_\mu) \right] J_{m_\nu}(kr_\mu) - kr_\mu y_\mu \sin(m_\nu \tilde{\theta}_\mu) J_{1+m_\nu}(kr_\mu), & \partial\Omega_1(\text{odd}) \\ m_\nu \left[-x_\mu \sin(m_\nu \tilde{\theta}_\mu) + y_\mu \cos(m_\nu \tilde{\theta}_\mu) \right] J_{m_\nu}(kr_\mu) - kr_\mu y_\mu \cos(m_\nu \tilde{\theta}_\mu) J_{1+m_\nu}(kr_\mu), & \partial\Omega_1(\text{even}) \end{cases} \tag{29b}$$

To calculate eigenvalues, one may absorb the factor r_μ^{-2} into the expansion coefficients since it is common to each term in the row.

In most of my examples, $A_2 = 1$ and $B_2 = 0$, but Neumann eigenvalues of the cut square shall also require $A_3 = 0$ and $B_3 = 1$.

Periodic-type edge (dihedral symmetry)

Next consider the periodic-type boundary conditions that arise if the geometry has dihedral symmetry. Although this analysis is rather elementary, it too seems to be rarely discussed in the context of this problem. Since the regular polygon[16] has dihedral symmetry, it will be used to most efficiently develop the matrix elements; but it also applies to another chosen shape, the 5-point star.

To that end, consider a σ-sided regular polygon (and other diagrams) shown in Fig. 5, with vertex angle $\beta = (\sigma - 2)\pi/\sigma$. The symmetry group of this shape is the dihedral group, D_σ, of degree σ or order 2σ. To work out the symmetry properties, first center the polygon at the origin with an apothem on the positive x-axis, as shown in Fig. 5 (LEFT). The dihedral group is generated by R, a counter-clockwise rotation by $\alpha = 2\pi/\sigma$, and Q, a reflection through the x-axis, i.e., $Q : y \to -y$.

The dihedral group has only 1-dim and 2-dim irreducible representations (irreps), so let η_1 and η_2 count those irreps. If σ is odd or even, then $\eta_1 = 2$ or $\eta_1 = 4$, respectively. Knowing η_1, we have $\eta_2 = (2\sigma - \eta_1)/4$. These 1-dim and 2-dim irreps lead to, respectively, non-degenerate and doubly-degenerate towers of eigenvalues.

---

[16] Although most of this analysis applies to all regular polygons, I shall exclude the closed-form solutions, as explained above.

Since $Q^2 = 1$, define a "Q-parity" such that any non-degenerate eigenfunction is either even or odd according to that parity. For the doubly degenerate pairs of eigenfunctions, one can always be made odd and the other even, and assume that this is done. Use a subscript to denote the Q-parity, as in

$$\varphi_e(x, -y) = +\varphi_e(x, y) \qquad \varphi_o(x, -y) = -\varphi_o(x, y) \qquad \text{Cartesian} \tag{30a}$$

$$\varphi_e(r, -\theta) = +\varphi_e(r, \theta) \qquad \varphi_o(r, -\theta) = -\varphi_o(r, \theta) \qquad \text{Polar} \tag{30b}$$

where "$\varphi(\mathbf{r})$" denotes a function in the regular polygon centered at the origin. An obvious but relevant fact is that all odd Q-parity functions are zero on the x-axis, i.e., $\varphi_o(x, 0) \equiv 0$.

For the regular polygon, the fundamental region may be chosen to be the shaded triangle of Fig. 5 (LEFT) because the entire polygon may be obtained from that triangle via group operations. Relevant to this project, it is a right triangle with two other angles

$$\frac{\alpha}{2} = \frac{\pi}{\sigma} \qquad \text{and} \qquad \frac{\beta}{2} = \frac{(\sigma - 2)\pi}{2\,\sigma}, \tag{31}$$

exactly one of which, $\beta/2$, is non-analytic (except for $\sigma = 3$, 4, and sometimes 6).

For the non-degenerate eigenfunctions, the triangular fundamental region becomes Ω. If σ is even, there are eight possible sets of edge conditions on this triangle since all its edges can be independently even or odd. But, if σ is odd, there are only four possible sets because the regular polygon's apothem must have the same symmetry as its circumradius (line connecting its center to a vertex).[17] When Ω is put in its canonical position, Fig. 5 (CENTER), it should become clear how to calculate the matrix elements for the non-degenerate eigenvalues.

For the doubly-degenerate eigenfunctions, we have an interesting choice. Since the group transformations form linear combinations of degenerate eigenfunctions, we may either (a) solve for *both* of the degenerate eigenfunctions within the fundamental region or (b) solve for *one* of the degenerate eigenfunctions in an area twice as large. In both cases, we can reconstruct both functions using the 2σ group transformations. Since choice (b) requires only one function, it shall be the better choice.

By reflecting the fundamental region about its hypotenuse to form the kite-shaped quadrilateral, we obtain the only polygon that is both twice as large and has (at most) one non-analytic vertex from which all edges can be seen. This kite quadrilateral thus becomes Ω for the doubly-degenerate eigenmodes.[18]

Cut this kite-quadrilateral out of the polygon as shown in Fig. 5 (LEFT), but before re-orienting it, observe that if we "rotate" the *even* Q-parity eigenfunction, we get the simple but important result that

$$\varphi_e(r, \alpha) = \cos(\gamma\alpha)\,\varphi_e(r, 0) \tag{32}$$

where $\gamma = 1, 2, ..., \eta_2$. The effective purpose of γ is to identify to which one of the η_2 doubly-degenerate eigenvalue towers this eigenfunction belongs.[19] (Note that this is where we used $\varphi_o(r, 0) \equiv 0$.)

That periodic-type symmetry relationship, Eq. (32), is useful because it relates values of an (even) eigenfunction on the positive x-axis (an apothem) to values of the same (even) eigenfunction on a neighboring apothem, i.e., at points P and P'.

When that kite quadrilateral is re-oriented to its canonical position, Fig. 5 (RIGHT), the apothems become point-matched edges and the regular-polygon boundary segments become adjacent edges; so that Eq. (32) gets transformed into

$$\Psi_e(k; r, \beta - \theta) = \cos(\gamma\alpha)\,\Psi_e(k; r, \theta), \tag{33}$$

where the even apothem becomes $\partial\Omega_2$. Note how the points P and P' are mapped. The subscript "e" is retained to remind us that we only need to consider this member of the degenerate pair to determine the eigenvalue tower.

Since the regular polygon is assumed to have either Dirichlet or Neumann boundary conditions, the adjacent edges ($\partial\Omega_1$ and $\partial\Omega_4$) are either both odd or both even. In this case, referring to Eq. (10), we can use

$$\sin(\nu\,(\beta - \theta)) = -(-1)^\nu \sin(\nu\,\theta) \tag{34a}$$

$$\cos((\nu - 1)(\beta - \theta)) = -(-1)^\nu \cos((\nu - 1)\,\theta) \tag{34b}$$

---

[17] This counting and the value of η_1 are related.

[18] The other obvious choice, the α-$\beta/2$-$\beta/2$ triangle, has *two* non-analytic vertices.

[19] To unify the expressions, one may include $\gamma = 0$ (all σ) and $\gamma = \sigma/2$ (even σ) for the even-parity, non-degenerate towers, but this is not done here because P' is not on the boundary of triangular fundamental region. It is easier to keep the solutions corresponding to 1-dim and 2-dim irreps separated.

to combine Eqs. (8) and (33), yielding,

$$0 = \sum_{\nu=1}^{N} c_\nu^{[N]} \left\{(-1)^\nu + \cos(\gamma\alpha)\right\} J_{m_\nu}(kr) \times \begin{cases} \sin(m_\nu\theta), & \partial\Omega_1(\text{odd}) \text{ and } \partial\Omega_4(\text{odd}) \\ \cos(m_\nu\theta), & \partial\Omega_1(\text{even}) \text{ and } \partial\Omega_4(\text{even}) \end{cases} \tag{35}$$

Evaluating this equation at each of the matching points on $\partial\Omega_2$ establishes $N/2$ equations for the N expansion coefficients; while the other $N/2$ equations are obtained by using the fact that $\partial\Omega_2$ is even. Requiring nontrivial solutions (for the expansion coefficients) leads to these $N/2$ rows of the point-matching matrix

$$\mathcal{M}_{\mu\nu}^{[N]}(\lambda) = \left\{(-1)^\nu + \cos(\gamma\alpha)\right\} J_{m_\nu}(kr_\mu) \times \begin{cases} \sin(m_\nu\theta_\mu), & \partial\Omega_1(\text{odd}) \text{ and } \partial\Omega_4(\text{odd}) \\ \cos(m_\nu\theta_\mu), & \partial\Omega_1(\text{even}) \text{ and } \partial\Omega_4(\text{even}) \end{cases} \tag{36}$$

while the other $N/2$ rows are obtained using the fact that $\partial\Omega_2$ is even.

There are really two point-matched edges, but that periodic-type boundary condition, Eq. (33), enables us to use one point-matched edge, twice. This requires that N be even, with $N/2$ points on edge $\partial\Omega_2$, and $N/2$ corresponding "phantom" points on $\partial\Omega_3$ which aren't actually numerically needed.

As it happens, the symmetry group of the star is D_5, i.e., the same as the regular pentagon. The fundamental region is a triangle with one non-analytic vertex (see Fig. 9), and the region Ω for the doubly degenerate eigenfunctions is an arrowhead quadrilateral (see Fig. 4), also with one non-analytic vertex—this time, a re-entrant vertex. To accommodate the star (and other polygons with dihedral symmetry), Eq. (36) is changed by replacing θ_μ with $\tilde{\theta}_\mu = \theta_\mu - \phi_1$, see Eq. (7).

As is common practice, the eigenfunctions can be identified by their nodal and antinodal patterns. With dihedral symmetry, the non-degenerate eigenfunctions have a maximal set of criss-crossing even and odd lines of symmetry. These are obtained by Riemann-Schwarz reflecting the eigenfunction within the triangular fundamental region to flesh out the full eigenfunction.

Every problem with such dihedral symmetry[20] will have at least two towers of non-degenerate eigenfunctions, here named the "symmetric" $\mathcal{S}$ and the "antisymmetric" $\mathcal{A}$, which have all even and odd lines of symmetry, respectively. If σ, as in "D_σ", is even, then there are two more non-degenerate symmetry classes that have lines of symmetry that alternate, even and odd, as one proceeds around the polygon. These might be named $\mathcal{S}'$ and $\mathcal{A}'$ according to even and odd Q-parity, respectively.

The doubly degenerate eigenfunctions can be similarly identified by the nodal and antinodal patterns since these functions have [at least] γ nodal *curves* crossing at the origin. Since the complexity of the nodal pattern increases with $\gamma = 1, 2, ..., \eta_2$; and we already used the symbol $\mathcal{A}$, label these η_2 symmetry classes using $\mathcal{B}$, $\mathcal{C}$, $\mathcal{D}$, ...; and when identifying a particular eigenfunction, suffix with an e or o to indicate Q-parity, as in $\mathcal{B}_e$ or $\mathcal{B}_o$.[21]

SOME NUMERICAL CONSIDERATIONS

When calculating the point-matching determinant, it is important that all calculations be carried out to relatively high precision. To get the process started, first calculate a low precision eigenvalue bound in order to estimate the convergence rate, ρ. Then use that to estimate the N-value targeting a high precision bound, accurate to, say, D digits, i.e., $N \leftarrow D/\rho$. To set the precision for this new calculation, use the rule-of-thumb requiring at least $1.2N$ digits in the intermediate calculations. If the process works, the precision was adequate. If not, try increasing it.

The roots of the determinant must certainly be found to a precision better than the desired D digits of the eigenvalue, perhaps to within $1.2D$ digits. I observed that for D beyond a few dozen digits, the point-matching determinant becomes quite linear in λ, so a simple secant-based root-finding algorithm works very well.

If one pursues hundreds of digits, the computer language must be able to handle arbitrary-precision calculations efficiently. Whatever programming environment you use, be sure that the numerics are good, especially the fractional-order Bessel functions.[22]

---

[20] Not just the regular polygons or the star. It is an exercise in geometry to figure out all of the specific shapes with dihedral-symmetry that also yield exponentially-convergent eigenfunction expansions (per the current procedure).

[21] Of course the division of eigenfunctions according to dihedral symmetry is hardly new. For example, Cureton and Kuttler [7] identify the symmetry classes for the regular hexagon, which can be lined up using $\mathcal{A} = S0$, $\mathcal{B}_e = S1$, $\mathcal{C}_o = S2$, $\mathcal{S}' = S3$, $\mathcal{S} = C0$, $\mathcal{B}_o = C1$, $\mathcal{C}_e = C2$, and $\mathcal{A}' = C3$; where the $S0$–$C3$ are class names in that reference.

[22] For example, and rather unfortunately, the `maxima` function `bessel_j` does not seem to respect `fpprec`.

EXAMPLES

My main project is the regular pentagon, for which I have so-far calculated the lowest 8139 Dirichlet eigenvalues to at least 60 correctly rounded digits. See Figs. 2 and 3 for several plots, including the highest one in that set; and—as presented in Table III—some hundred-digit eigenvalue results. Except for those examples, I find it more interesting to use other shapes to demonstrate the eigenvalue calculation and bounding methods.

L-shape

This project would not be complete without considering the famous L-shape formed by joining two unit-edged squares to adjacent edges of a third, as shown in Fig. 6. For this, I shall limit the scope to calculating the lowest Dirichlet eigenvalue. The first one-hundred digits of this eigenvalue appear in Table III, and an abbreviated bound is

$$\lambda_1 = 9.6397238440219410527 \cdots 2749461005701606185 8^{5300}_{4831} \tag{37}$$

where the leading and trailing digits of the 1001-digit result are shown. The first 1001 decimal digits of this number are listed as http://www.oeis.org/A262701 [17].

The 2004 influential "Reviving the Method of Particular Solutions" by Betcke and Trefethen [5], which, among other things, examines the L-shape as an example, and apparently provides the best modern reference for this shape. Despite that, I regress back to 1967 and use FHM as a starting point.
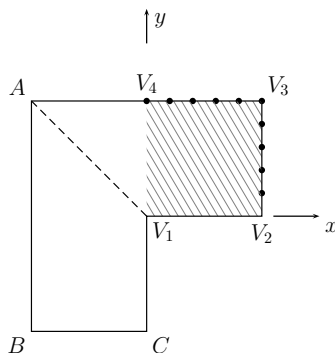

FIG. 6. L-shape showing a line of symmetry (even line $V_1 A$) and region Ω (shaded square $V_1 V_2 V_3 V_4$, in its canonical position) with ten evenly-spaced matching points.

Following FHM, fully exploit symmetry to yield a square region, Ω, in its canonical position as shown by the shaded region of Fig. 6. This means we can use Eq. (8) with m-values

$$m_\nu = \frac{2}{3} \left(2 \left\lfloor \frac{3\nu}{2} \right\rfloor - 1 \right) \tag{38}$$

where $\lfloor x \rfloor$ is floor(x). The expression in parentheses gives the required sequence $\{1, 5, 7, 11, 13, ...\}$; i.e., (positive) integers on either side of the integers in $\{0, 6, 12, ...\}$, which are appropriate for the lowest Dirichlet eigenmode.

Now, consider a near repeat of the FHM calculation for an "apples-to-apples" comparison—this time using arbitrary precision and much higher N-values. To do this exercise, (a) choose equally-spaced matching points on $\partial\Omega_2$ and $\partial\Omega_3$; (b) impose $\partial\Psi(k; r, \theta)/\partial\theta = 0$ at V_2 and V_3; and (c) use the proper increment of $\Delta N = 2$. Then, to numerically verify the alternating/converging nature, calculate every approximate eigenvalue for even N from 4 to just over 260.[23] The results for $N = 4, 6, ..., 32, 254, ..., 260$ are shown in Table I, which illustrates the alternation.

FHM reported the eight-digit 9.6397238^{84}_{05} (FHM Table 3) eigenvalue bound, and they indicate calculations up to $N = 26$ (FHM Table 2). FHM round-off error appears to become significant for $N > 14$, so use my very low-order $N = 12$ and 14 numbers for that "apples-to-apples" comparison. By inspection, the bound is 9.6397238^{55}_{43}. This happens to be slightly better, but the emphasis should be placed on the ease with which this bound is obtained.

---

[23] That highest N value yields 100 correct digits in the eigenvalue, and altogether, takes about one hour of CPU time. Also note that requirement (b) was imposed by FHM for numerical reasons, I impose it here to accurately reproduce their results.

Interestingly, FHM data is essentially the same as mine out to ninth decimal place, so that original FHM ($N = 12$ and 14) data might be used to bound the eigenvalue to around eight digits without using Moler-Payne, however, without more precision and higher N-values, it is not obvious that the alternation may be used to bound the eigenvalue. Note that the N-value used in the FHM Moler-Payne calculation was not indicated.

TABLE I. Very low-order and a few high-order results for the L-shape using the FHM procedure. At least five digits after the last matching digit are retained and rounded, and the underlined digits guide the eye. Note the alternation: Very consistently, even and odd $N/2$ provide, respectively, upper and lower bounds. The last few entries indicate a 100-digit calculation (ending in "...788"), with the last three showing how to construct the bound. FHM Table 2 data are copied here for side-by-side comparison.

N	λ	FHM λ^*
4	9.6̲58161723	9.658161723
6	9.639̲624491	9.639624491
8	9.6397̲266319	9.639726632
10	9.63972̲370221	3703
12	9.639723̲854826	3855
14	9.6397238̲430369	3844
16	9.63972384̲412442	3844
18	9.639723844̲010281	3845
20	9.6397238440̲233611	3845
22	9.63972384402̲175875	3845
24	9.639723844021̲965466	3844
26	9.639723844021̲937668	3846
28	9.6397238440219̲415358	
30	9.6397238440219̲409820	
32	9.63972384402194106̲3271	
$\vdots$		
254	9.6[$\cdots$]50087967̲864481	
256	9.6[$\cdots$]50087967̲892906	$(\cdots 78\,^{93}_{64})$
258	9.6[$\cdots$]5008796788̲742560	$(\cdots 78\,^{93}_{87})$
260	9.6[$\cdots$]5008796788̲848247	$(\cdots 788\,^{85}_{74})$

Except for the P. Amore et al. [1] recent effort, I believe the best published result is the decade-old, 13-digit correctly rounded result of Betcke and Trefethen [5], $9.63972384402\,^{22}_{16}$. To make a reasonable comparison, they used the GSVD method, no symmetry reduction, $240 = 4 \times 60$ equal-spaced boundary matching points (excluding all vertices) on four point-matched segments, 50 randomly-selected interior points, only 15 basis-functions, and machine-precision. That required minimizing the smallest generalized singular value of a $(50 + 240) \times 240$ matrix and (to obtain the MP-type bounds) estimating the function values on the point-matched edge.

Using the current method, which has a better distribution of points (by including vertices and actually being evenly spaced) and taking full advantage of symmetry, a similar looking bound $9.63972384402\,^{34}_{17}$ is achieved by comparing the $N = 20$ and 22 approximate eigenvalues. This result required a few seconds of CPU time. Although not an "apples-to-apples" comparison, it does indicate significantly less numerical effort is required to obtain a similar result.

Next, I extend the calculations from $N = 814$ up to 826, still using equally-spaced matching points[24], to obtain a 300-digit result with an overall convergence rate of $1/2.75$. This took about a day of CPU time.

Then, I switched to Chebyshev-distributed points (very similar to those shown in Fig. 8 for the cut-square), which improved the convergence rate to very close to $1/2$. This allowed calculation of a 400-digit result at a similar $N = 816$, after another CPU day. By extending N-values up to about 2100, "thousand-digit" results may be obtained after several weeks of CPU effort. This illustrates how exploiting symmetry and judiciously choosing matching points permits one to extend results to very high precision.

---

[24] ... but abandoning the $\partial \Psi / \partial \theta = 0$ requirement at V_2 and V_3

Cut-square

The sole and limited purpose of this example is to illustrate the bounding method for the apparently difficult shape shown in Fig. 8, which I call the "cut square" since it is formed by cutting a triangle out of a unit-edged square. It has six edges and a $7\pi/4$ re-entrant vertex. It was inspired entirely by an example in Reference [21]. Those authors, Yuan and He, were apparently unaware of the then-recent relevant work by Trefethen and Betcke [5, 20], but nevertheless provide an interesting discussion on the L-shape and this cut-square shape—as they attempt to bound eigenvalues. Of note is that those authors point out that this shape has no symmetry, but indeed it does.[25]
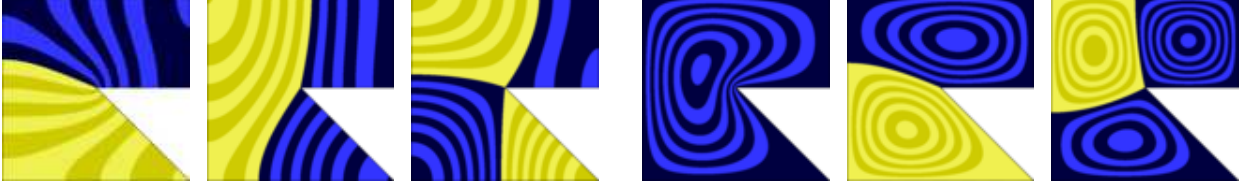
FIG. 7. Example contour plots. Blue and yellow areas are opposite sign, and light-dark steps indicate level contours. These are (LEFT) the lowest three Neumann and (RIGHT) the lowest three Dirichlet eigenfunctions. Their eigenvalues are listed in Table III, and they are not degenerate.

For this polygon, calculations of both Dirichlet and Neumann eigenvalues are demonstrated. Because of the very high convergence rate of $\rho \approx 1/2$, with modest effort, the lowest three eigenvalues for each type are calculated to 200 digits, with 100-digit truncated values presented in Table III.

The first challenge is to identify the symmetries and classify the eigenmodes. To do this, first consider the Dirichlet modes and expand the eigenfunction (Eqs. 8 and 9, choosing "sin") about the re-entrant vertex with

$$m_\nu = \frac{4\nu}{7} \qquad \text{where } \nu = 1, 2, 3, ..., N. \tag{39}$$

By calculating the eigenfunction coefficients (the c_ν in Eq. (8)), a pattern is revealed where, for a given eigenfunction, many coefficients are zero. That lead to a simple discovery[26] of a symmetry quite analogous to that of the L-shape. By inspection of the calculated coefficients, it became obvious that (a) closed-form modes are selected by choosing integral m, while (b) any non-closed-form eigenmode belongs to one of three classes (here labeled A, B, and C) obtained by choosing positive ν-values on either side of multiples of seven. To best reveal the pattern, line up the possible m-values,

$$m = [0,] \overset{A}{\tfrac{4}{7}}, \overset{B}{\tfrac{8}{7}}, \overset{C}{\tfrac{12}{7}}, \overset{C}{\tfrac{16}{7}}, \overset{B}{\tfrac{20}{7}}, \overset{A}{\tfrac{24}{7}}, 4, \overset{A}{\tfrac{32}{7}}, \overset{B}{\tfrac{36}{7}}, \overset{C}{\tfrac{40}{7}}, \overset{C}{\tfrac{44}{7}}, \overset{B}{\tfrac{48}{7}}, \overset{A}{\tfrac{52}{7}}, 8, \overset{A}{\tfrac{60}{7}}, \cdots \tag{40}$$

where the zero is shown but used only for the closed-form Neumann solutions.

The fundamental region for the closed-form modes appears to be the 45-90-45 triangle. However, the smallest region in which I can solve the problem for the non-closed-form classes appears to be twice as large, 2/7 of the total area, which can be chosen to be the square region in the first quadrant. Thus, for the non-closed-form modes, there are two point-matched edges meeting at right angles—as with the L-shape.

I found that a Chebyshev-like distribution of matching points, equally divided between the two matching edges on the square in the first quadrant, and crowded near the 90-degree corners (V_2 and V_3), yields excellent convergence rates. Because of these choices, N must be even, and very specifically,

$$\mathcal{P}_N : (x_\mu, y_\mu) = \begin{cases} \left(\dfrac{1}{2}, \dfrac{1}{4} \left[1 - \cos\left(\dfrac{[\mu - \frac{1}{2}]}{N/2} \pi \right) \right] \right) & \text{for} \quad \mu = 1, 2, \cdots, \frac{N}{2} \\ \left(\dfrac{1}{2} \sin\left(\dfrac{[\mu - \frac{1}{2}]}{N} \pi \right), \dfrac{1}{2} \right) & \text{for} \quad \mu = \frac{N}{2} + 1, \frac{N}{2} + 2, \cdots, N \end{cases} \tag{41}$$

Incrementing μ, these matching points start near V_2, and end near the midpoint of V_3 and V_4, as shown in Fig. 8.

---

[25] Very recently, P. Amore et al. [1] also examined this shape and discovered other interesting symmetry properties, and were also able to calculate very precise Dirichlet eigenvalues. They reported 40-digit MPS results, which do agree with my results.

[26] This generally identifies a clever technique that can be used to empirically discover symmetries if they are not obvious or one is not inspired to figure it out from first principles. FHM has indications of this technique.
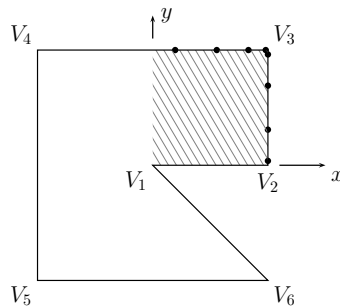
FIG. 8. Cut-square hexagon and example $N = 8$ matching points (N even and $N/2$ on each edge, as shown). There are two matching points very close to vertex V_3 (one on each edge), and one very close to vertex V_2. The shaded region is the most convenient and smallest Ω region needed to solve for the non-closed-form eigenvalues.

A sweep of the interval from $\lambda = 0$ to 100 reveals the first three Dirichlet eigenvalues, which belong to class A, B, and C; respectively. Initial bounds (within ±1) of these three are $\lambda_1 = 36$, $\lambda_2 = 54$, and $\lambda_3 = 74$; which are then calculated to 200 digits, with 100-digit truncated values presented in Table III. The lowest closed-form Dirichlet eigenvalue[27] is relatively high at $\lambda \approx 197.4$, which appears to be the tenth Dirichlet eigenvalue.

The discussion for the Neumann modes is nearly identical, except that one must choose "cos" (in Eq. 9) and, for the closed-form modes, one must include the $m = 0$ term. Also, this example is unique among the chosen examples because there are two even point-matched edges.

Like the Dirichlet results, the lowest three Neumann eigenvalues belong to symmetry classes A, B, and C; respectively. They are initially bounded (within ±1) with $\lambda_1 = 5$, $\lambda_2 = 12$, and $\lambda_3 = 18$; which are then calculated to 200 digits, with 100-digit truncated values presented in Table III. The lowest closed-form Neumann eigenvalue[28] is $\lambda \approx 39.5$, which is apparently the next one up.

For these lowest Neumann and Dirichlet eigenvalues, the convergence rate is quite rapid at about $1/2$, which means about 400 matching points are needed to yield the 200-digit results.

Prior to this work and that of Ref. [1], the only published eigenvalue for this shape was the lowest Dirichlet eigenvalue, and the best bound is the six-digit result, $\lambda_1 = 35.6315\,^{22}_{15}$. To get that, Yuan and He [21] used a similar MPS starting point, fifty matching points in total on all but the two adjacent edges forming the "cut", and a far more complicated bound calculation. (Their distribution of points was unspecified.) To obtain an "apples-to-apples" comparison with that publish result, I temporarily abandoned the symmetry considerations and repeated the calculation for up to the relatively low $N = 49$ matching points (using N—a multiple of seven—Chebyshev matching points, distributed on all four non-adjacent edges), and was able to write down a nine-digit estimate $\lambda_1 = 35.6315195\,^{37}_{15}$, by inspection. That "low-precision" result took a few seconds of CPU time.

It is interesting to note that by simply restoring the symmetry reduction, the convergence rate becomes about three times faster: At 50 expansion terms (i.e., the same numerical effort, requiring a few CPU seconds), I can write down thirty digits, $\lambda_1 = 35.63151951\,7191723095\,2054861420\,^{79}_{61}$, again, by inspection.

In hindsight, this problem was not as difficult (to solve) as one might have been led. But there are interesting features that do suggest further research, such as the nature of the symmetry.

Star (regular concave decagon)

The five-pointed star provides another relatively difficult shape with which to demonstrate the method. It is also known as a regular concave decagon or the outline of the pentagram star. The size is such that points of the star coincide with the vertices of a unit-edged, regular pentagon.

This shape shares the same symmetry group as the regular pentagon. Since I observed some regular-pentagon Dirichlet eigenfunctions develop nodal lines approximating a regular *pentagram*—two examples are illustrated in Figs. 2d and 3b; I was inspired to examine this shape, at least for a few low eigenvalues.

A subset of eigenmodes of the regular pentagon do have an approximate symmetry leading to that observation, however, I reserve that for a future discussion. This star can become a research project in and of itself: It is an interesting and familiar shape for which I have been unable to find any published eigenvalues for comparison.

---

[27] $\lambda = (1^2 + 2^2)(\pi/L)^2 = 20\pi^2 \approx 197.4$, where $\Psi(x,y) \propto \sin(\pi x/L)\sin(2\pi y/L) - \sin(2\pi x/L)\sin(\pi y/L)$ and $L = 1/2$. Not degenerate.

[28] $\lambda = (1^2 + 0^2)(\pi/L)^2 = 20\pi^2 \approx 39.5$, where $\Psi(x,y) \propto \cos(\pi x/L) + \cos(\pi y/L)$ and $L = 1/2$. Not degenerate.
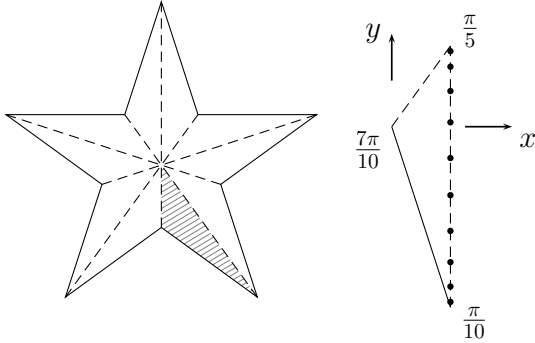
FIG. 9. (LEFT) Star shape with all even lines connecting opposite vertices and (RIGHT) the fundamental region forming the polygon, Ω, in its canonical position and with $N = 10$ Chebyshev-like distributed matching points.
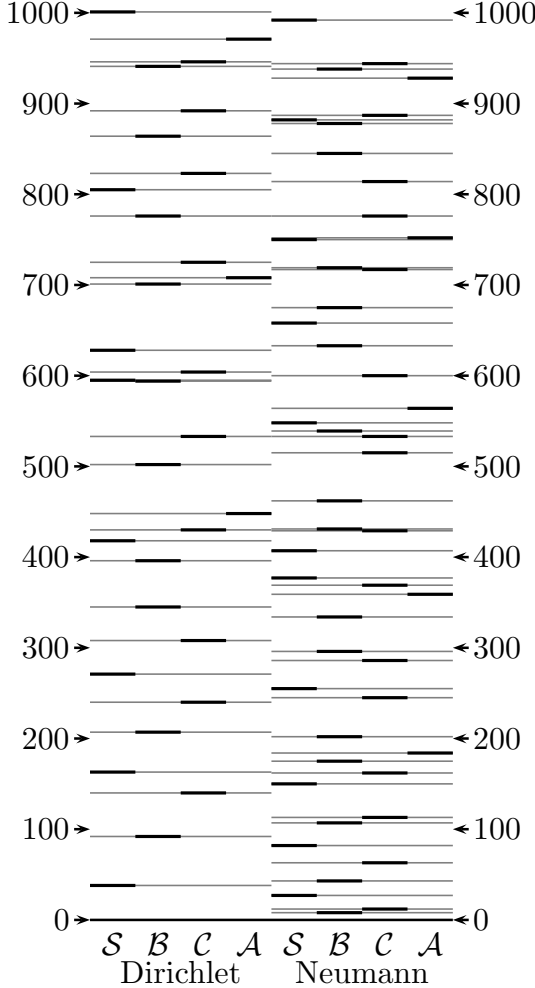

FIG. 10. The spectrum of the concave decagon (star) for $\lambda < 1002$. This diagram includes the lowest 79 eigenvalues, which is composed of 31 Dirichlet and 48 Neumann eigenvalues. They are sorted according to symmetry. Except that every B and C eigenvalue is doubly degenerate, there are actually no other degeneracies in this set—even though some come close.

Like the regular pentagon, all star eigenvalues can sorted into one of two one-dimensional or two two-dimensional classes. The non-degenerate $\mathcal{S}$ and $\mathcal{A}$ eigenvalues require the triangular fundamental region shown in Fig. 9. The doubly-degenerate $\mathcal{B}$ and $\mathcal{C}$ "mixed" modes require the arrow-head shape shown in Fig. 4, which is formed by reflecting the fundamental triangle through it shortest edge.

With this problem, unlike some other examples, I could not get the point-matching method to converge with evenly-

spaced matching points, however, it does work with points crowded near the vertices. A distribution that yields good convergence rates is the Chebyshev-like distribution

$$y_\nu = \frac{1}{2} \left\{ [y_C + y_B] + [y_C - y_B] \cos\left(\frac{\nu\pi}{n_2 + 1}\right) \right\} \tag{42}$$

for $\nu = 1, 2, ..., n_2$; where $n_2 = N$ ($\mathcal{A}$, $\mathcal{S}$) or $N/2$ ($\mathcal{B}$, $\mathcal{C}$), and where y_B and y_C are the y-values of the matching-edge endpoints. With this distribution, there is not a simple alternation of approximate eigenvalues with incremented values of N. Instead, it usually takes several (about three) steps to alternate. The convergence rate is nevertheless high enough that the peaks can be interpreted as upper and lower bounds.

The lowest seventy-nine eigenvalues (including both Dirichlet and Neumann modes) were calculated for $\epsilon < 10^{-20}$, and since so little is known about this problem, the rich spectrum is simply and concisely presented in Fig. 10. Several representative eigenfunctions are presented in Fig. 2, and the lowest four Dirichlet and lowest four Neumann eigenvalues are calculated to at least 100 digits and presented in Table III.

Regular polygons

Of the regular polygons, it is well known that the equilateral triangle and the square are fully solved in closed form, and the regular hexagon has a subset of closed-form solutions (by piecing together equilateral triangle solutions). Otherwise, regular polygons have no closed-form solutions.

Quite surprisingly, (non-closed-form) regular polygon results are rather fragmentary and spread far and wide in the published literature. This represents a gaping hole in our collective understanding.

To illustrate, consider the regular hexagon. In 1978, Bauer and Rice [4] calculated the lowest 21 Dirichlet eigenvalues to at least five or so digits. In 1993, I [11] extended that by a factor of three, to about six digits; and in 1998, Cureton and Kuttler [7] almost doubled that tally, and to about eight digits.

The regular pentagon is no better. In 2010, Lanz [13] published what appears to be the most comprehensive list (that I am aware of) consisting of the ten lowest Dirichlet eigenvalues, accurate to half-a-dozen digits.

Jumping to the more extreme 128-sided regular polygon: In 2004, Strang and Grinfeld [18], and in 2008, Guidotti and Lambers [10], both calculated the ten lowest simple Dirichlet eigenvalues, accurate to about half-a-dozen digits, the lowest of which ranges from 5.78319 to 5.78320 (adjusting for the area). In addition, those authors, and—more specifically—Oikonomou [16], offer an asymptotic expansion in "$1/\sigma$" where σ is the number of sides on the regular polygon. Recently, Mark Broady[29] [6] added two more terms to that expansion, which, for the lowest Dirichlet eigenvalue, is

$$\frac{\lambda_1}{j_{0,1}^2} = \left\{ 1 + \frac{4\,\zeta(3)}{\sigma^3} + \frac{\left[12 - 2\,j_{0,1}^2\right]\,\zeta(5)}{\sigma^5} + \frac{\left[8 + 4\,j_{0,1}^2\right]\,\zeta^2(3)}{\sigma^6} + \mathcal{O}\left(\frac{1}{\sigma^7}\right) \right\}. \tag{43}$$

where the regular polygon has area equal to π, $j_{0,1} \approx 2.4048$ is the first root of the Bessel function $J_0(x)$, and $\zeta(x)$ is the Riemann-zeta function.[30] Incidentally, and as far as I know, that has been the only effort to express any non-closed-form eigenvalues analytically in terms of other "known" constants.

To illustrate the method, I find it interesting to calculate the lowest Dirichlet eigenvalues of σ-sided regular polygons with up to $\sigma = 130$ at a precision of $\epsilon < 10^{-30}$. The tail end of that calculation is shown in Table II, with truncated 100-digits results for the pentagon to the decagon presented in Table III. See also Eq. (21) for a 20-digit result for the 256-sided regular polygon, which was used to illustrate the notation.

Of note is that above the dodecagon, i.e., $\sigma > 12$, the canonical Chebyshev distribution given by Eq. (23) doesn't work. Instead, using half of it does seem to work for all regular polygons,

$$y_\nu = y_{max} \sin(\nu\pi/(N+1)) \tag{44}$$

where $\nu = 1, 2, ..., N$, and where y_{max} is the y-value of the highest point of the fundamental triangle in Fig. 5 (CENTER); here $y_{max} = \cos(\pi/\sigma)$. This distribution crowds matching points near the "distant" acute angle ($\alpha/2 = \pi/\sigma$), and spreads them out near the right angle. It also seems to very reliably yield alternating approximations at each increment, $\Delta N = 1$.

---

[29] Private communication.
[30] Area-π regular polygons are preferred since it factors out the well-known area dependence on the eigenvalue; and, as $\sigma \to \infty$, $\lambda_1 \to j_{0,1}^2$.

This exercise illustrates specifically that even though exponential convergence is present, as the number of sides increases, the convergence rate becomes quite poor. Beginning at the pentagon, $\rho \approx 1/1.14$ when $\epsilon \approx 10^{-1000}$. When one reaches the 130-sided regular polygon, that convergence rate has dropped to about $\rho \approx 1/28.1$ at the 30-digit result. A rough estimate for the convergence rate for this problem is $\rho \approx 5/\sigma$, at least for the 30-digit results.

Also of note is that when the convergence rate is good, more precision in the calculations is needed: The regular pentagon required $1.7N$ digits. Above the decagon, $1.4N$ seemed adequate.

For situations where σ (number of polygon sides) is low (5 or 6), with a little practice, it becomes relatively straightforward to calculate hundred-digit results, for both Neumann and Dirichlet boundary conditions, for up to perhaps the lowest ten thousand eigenvalues. For example, the 8139th Dirichlet eigenvalue (same symmetry class as the lowest) of the (unit-edged) regular pentagon to 300 correct digits is bound with

$$\lambda_{8139} = 100001.28198274831240\cdots32644630143129793681^{5381}_{3271} \tag{45}$$

which, as indicated, displays the leading and trailing digits.

Turning attention to how far one can extend the precision of these numbers using a laptop, two "1000+" digit eigenvalues are calculated. The lowest Dirichlet eigenvalue of the unit-edged regular pentagon, to 1502 digits,

$$\lambda_1 = 10.996427084559806648\cdots82166474404544652968^{9936}_{8251} \tag{46}$$

was submitted to `http://www.oeis.org/A262823` [17]. This hexagon number required just under one month of computation time.

Similarly, the lowest Dirichlet eigenvalue of the unit-edged regular hexagon, to 1001 correct digits,

$$\lambda_1 = 7.1553391339260551282\cdots77979918378681828158^{1503}_{0889} \tag{47}$$

was submitted to `http://www.oeis.org/A263202` [17]. This required about five days of computation time.

TABLE II. Thirty-digit results for the lowest Dirichlet eigenvalue within a regular polygon with number of sides σ and area π. The last entry is $j_{0,1}^2$, i.e., the corresponding eigenvalue of the unit-radius circle. Note how the required number of matching points, $\widehat{N}$, increases by about six each time to maintain the desired eigenvalue precision. Each of these polygon eigenvalues required about a day of CPU.

σ	λ_1 ($\epsilon < 10^{-30}$)	$\widehat{N}$	ϵ
126	$5.78319986391698116979559972755^{5287}_{4738}$	818	9.5×10^{-31}
127	$5.78319953812368041217455201387^{147}_{6591}$	824	9.6×10^{-31}
128	$5.78319922243209895698523832013^{555}_{030}$	831	9.7×10^{-31}
129	$5.78319891645372682901545245421^{643}_{112}$	837	9.2×10^{-31}
130	$5.78319861981784749432269771828^{587}_{013}$	842	9.9×10^{-31}
∞	$5.78318596294678452117599575845 6$		

CONCLUSION

By using a method substantially identical to that of FHM, but using modern hardware and [free] software, and a little patience, I have demonstrated that it becomes relatively easy to exploit the well-known "exponential convergence" to calculate eigenvalues of the Laplacian to very high precision, very typically hundreds of digits, and about a thousand digits for the lowest Dirichlet eigenvalue of the L-shape (1001 digits), regular pentagon (1502 digits), and regular hexagon (1001 digits).

I believe my unique contribution to this problem includes (a) the observation that the sequence of approximate eigenvalues alternates as one adds matching points—thus yielding an easy and excellent method to bound eigenvalues, (b) revealing a very simple way to overcome the numerical ill-conditioning of the point-matching method and exploit its advantages to permit easy calculation of those eigenvalues, and (c) computing the first hundred-digit and thousand-digit non-closed-form eigenvalue results for a variety of shapes.

As I explore this interesting and classic problem, I see theoretical and pedagogical gaps that need to be filled, and a need to compile results. My hope is to inspire others pick a shape and start calculating.

APPENDIX

TABLE III. Selected ultra-precise eigenvalues for the shapes shown in Fig. 1. Each line has 100 digits in groups of ten. Many of these eigenvalues have been calculated to significantly higher precision, but all are truncated here to 100 digits. All of these reported digits are believed to be correct.

Lowest Dirichlet eigenvalue of the L-shape (OEIS/A262701)
9.6397238440 2194105271 1459262364 8231562672 8952582190 6456109579 7005640356 4786337039 0722873165 008796788
Lowest three Dirichlet eigenvalues of the cut-square
35.63151951 7191723095 2054861420 7765698409 6719323704 4187565934 6885272248 0828423119 6945786239 3580027104
54.19310844 4246291974 1197858564 7040768914 7834351054 6172416365 9816279545 9613641230 6675978946 4088833202
73.63330812 5603834594 8382867456 6950026083 7320383040 6422202112 5756253401 4601480363 5503338306 9092168350
Lowest three Neumann eigenvalues of the cut-square
4.8725276926 5604412939 9958456263 8223244356 0835019173 6918287660 7254479092 9224360057 0084074146 2382445186
11.68901246 7975646418 5606630328 8745685066 8757229760 0410850473 2248922177 2876660771 9335431729 8467748934
18.41355366 4057643462 4365786419 2874654908 0932393352 2677244373 5428238912 2726711980 3455782771 2026452147
Lowest four Dirichlet eigenvalues of the star
38.16467784 9021956120 7064401254 4909302761 7878759405 6032173115 9893430940 1381888098 1660705230 8934649411
91.52297660 0087650110 1874055059 4495578448 7274004759 3637987954 9616910512 9744672654 0219433040 9841939843
140.1751508 7431829715 7695648583 4562984886 8950461859 0551648700 0199831865 5965928820 7377894288 1434147089
163.1376917 3762835226 6351068194 6753674371 1941271352 4052991614 0611124064 5716586029 2880248852 0079395340
Lowest four Neumann eigenvalues of the star
8.1427909641 2194647234 7929848146 9295230245 4007315742 8138507177 5037804202 8718792913 7927332910 03542992
12.39876832 7444927056 0165051825 7451412024 6307375894 2540568120 9312929258 9363195125 1866820544 1275209247
27.35593497 9775790508 6023809638 0191310466 0644900698 7296023165 9815796111 1183248158 1641731648 2599322915
43.45373653 4633280721 7484231722 7400872562 0705962339 9821299710 0656883686 6791890220 6208479355 9294072629
Lowest Dirichlet eigenvalue of regular polygons (area=π), sides $\sigma = 5, 6, 7, 8, 9, 10$
6.0221379320 4263387829 8008710054 2429670053 0534044855 7980207884 6736673784 8013486862 2358041642 6117672672
5.9174178316 1366121568 8574457683 8961545008 2860040929 3411904080 5009620004 4903613632 2387404110 3755146850
5.8664493126 5559858577 1247494175 8841084242 7349136980 5378445601 2986066686 0112738387 6297693674 2836505116
5.8384914335 9244285051 6640379563 8157848367 5715202596 2094176052 5251139412 6946260372 4227921796 5891515...
5.8218268022 7026573175 5464437169 4592167178 6764620589 1079251159 2184091668 2976322605 9528552020 2545987984
5.8112603592 1911602278 8816468811 1646234421 5817490023 1913274885 8828042612 9402097114 1604226529 2694626...

[1] P. Amore, J. P. Boyd, F. M. Fernandez, and B. Rosler. High order eigenvalues for the Helmholtz equation in complicated non-tensor domains through Richardson Extrapolation of second order finite differences. 2015. http://arxiv.org/abs/1509.02795.

[2] Alex Barnett and Andrew Hassel. Fast computation of high frequency Dirichlet eigenmodes via spectral flow of the interior Neumann-to-Dirichlet map. *Comm. Pure Appl. Math.*, 67(3):351–407, 2014. More recent reference to MPSpack.

[3] Alex H. Barnett and Timo Betcke. An exponentially convergent nonpolynomial finite element method for time-harmonic scattering from polygons. *SIAM J. Sci. Comp.*, 32(3):1417–1441, 2010. Quote: "MPSpack is an object-oriented MATLAB toolbox developed by the authors to solve two-dimensional Helmholtz/Laplace PDE problems with particular and fundamental solution methods. The code can be obtained from http://code.google.com/p/mpspack.

[4] L. Bauer and E. L. Reiss. Cutoff wavenumbers and modes of hexagonal waveguides. *SIAM J. of Appl. Math.*, 35:508–514, 1978.

[5] Timo Betcke and Lloyd N. Trefethen. Reviving the method of particular solutions. *SIAM Rev.*, 47:469–491, 2004.

[6] Mark Boady. *Applications of Symbolic Computation to the Calculus of Moving Surfaces*. PhD thesis, Drexel University, Philadelphia, PA, 2015.

[7] L. M. Cureton and J. R. Kuttler. Eigenvalues of the Laplacian on regular polygons and polygons resulting from their dissection. *Journal of Sound and Vibration*, 220:83–98, 1998.

[8] L. Fox, P. Henrici, and C. Moler. Approximation and bounds for eigenvalues of elliptic operators. *SIAM J. Numer. Anal.*, 4:89–102, 1967.

[9] Torbjörn Granlund and the GMP development team. *GNU MP: The GNU Multiple Precision Arithmetic Library*, 6.0.0 edition, 2015. Available online `http://gmplib.org/`.

[10] P. Guidotti and J. V. Lambers. Eigenvalue characterization and computation for the Laplacian on general 2-D domains. *Numerical Functional Analysis and Optimization*, 29:507–531, 2008.

[11] R. S. Jones. *The one-dimensional three-body problem and selected waveguide problems: solutions of the two-dimensional Helmholtz equation*. PhD thesis, The Ohio State University, 1993. NOTE: In that early effort to numerically solve the non-closed-form, 30-60-90 triangle solutions, I incorrectly expanded around the analytic 30° vertex.

[12] J. R. Kuttler and V. G. Sigillito. Eigenvalues of the Laplacian in two dimensions. *SIAM Rev.*, 26:163–193, 1984.

[13] Colleen Lanz. The use of Schwarz-Christoffel transformations in determining acoustic resonances. Master's thesis, Virginia Polytechnic Institute and State University, 2010.

[14] Maxima. *Maxima, a Computer Algebra System. Version 5.31*. http://maxima.sourceforge.net/, 2015.

[15] C. B. Moler and L. E. Payne. Bounds for eigenvalues and eigenvectors of symmetric operators. *SIAM J. Numer. Anal.*, 5:64–70, 1968.

[16] V. K. Oikonomou. Casimir energy for a regular polygon with Dirichlet boundaries. 2010. `http://arxiv.org/abs/1012.5376`.

[17] N. J. A. Sloane. *The On-Line Encyclopedia of Integer Sequences*, 2010. Published electronically at `http://oeis.org`.

[18] G. Strang and P. Grinfeld. The Laplacian eigenvalues of a polygon. *Computers and Mathematics with Applications*, 48:1121–1133, 2004.

[19] The PARI Group, Bordeaux. *PARI/GP version* `2.7.3`, 2015. Available online `http://pari.math.u-bordeaux.fr/`.

[20] Lloyd N. Trefethen and Timo Betcke. Computed eigenmodes of planar regions. *Contemp. Math., Amer. Math. Soc.*, 412:297–314, 2006.

[21] Quan Yuan and Zhiqing He. Bounds to eigenvalues of the Laplacian on L-shaped domain by variational methods. *J. Comp. Appl. Math.*, 233:1083–1090, 2009.